Sensors and Materials, Vol. 34, No. 5 (2022) 1909–1916
MYU Tokyo

S & M 2941

Self-powered Fault Diagnosis Using Vibration Energy Harvesting and Machine Learning

Tomohiro Sato, Mitsuki Funato, Kiyotaka Imai, and Takashi Nakajima*

Department of Applied Physics, Faculty of Science, Tokyo University of Science,
6-3-1 Niijuku, Katsushika, Tokyo 125-8585, Japan

(Received March 30, 2022; accepted April 8, 2022)

Keywords: energy harvesting, vibration, piezoelectrics, machine learning, edge device

In this work, a self-powered fault diagnosis system using vibration energy harvesting was constructed to verify the accuracy of state identification and abnormality detection for a monitored target. A vibration energy harvester and a sensor were attached to an air compressor to be monitored, and the sensor signal was transmitted wirelessly using the energy acquired. Using the supervised machine learning of the *k*-nearest neighbor algorithm with the vibration sensor signal and the wireless transmission interval, the algorithm was able to identify three states (normal, unstable, and overturned) with a maximum accuracy of 99%. In addition, by using the local outlier factor algorithm as unsupervised learning, it was possible to achieve abnormality detection with a maximum accuracy of 98%. The accuracy of fault diagnosis was improved by analyzing not only the sensor signals but also the wireless transmission interval as machine learning features. It was found that the frequency of wireless transmission by energy harvesting is valuable information for determining the status of the monitored target.

1. Introduction

Technology related to energy harvesting, in which the energy in the environment is acquired and utilized as electrical energy, is attracting attention.[1] This is due to the dramatic increase in the number of sensors in society, as symbolized by the trillion-sensor society. It is difficult to power these sensor nodes only with batteries, which need to be recharged and replaced, and energy harvesting is becoming inevitable. In such a large sensor network, the sensors must operate over a long period of time without the need for human maintenance.[2–4] Therefore, a number of studies have been conducted to overcome the research challenges in this area. Several methods of energy harvesting that are powered by vibrations,[5–8] heat,[9–11] sunlight,[12,13] and electromagnetic waves[14,15] have been developed. However, the power that can be acquired through energy harvesting is limited to about μW–mW,[16] and the time available to operate wireless devices and sensors is finite.[17–19] This means that the number of data that can be transmitted is very small, and it is also difficult to transmit data continuously. Under these circumstances, improving the accuracy of diagnosis in a constant monitoring system powered by energy harvesting is an important research issue.

*Corresponding author: e-mail: nakajima@rs.tus.ac.jp
https://doi.org/10.18494/SAM3907

ISSN 0914-4935

Against this background, the purpose of this study was to establish a system that can diagnose anomalies with high accuracy when the transmitted information is sparse due to the limited energy. Notably, a diagnostic algorithm based on machine learning was incorporated to detect and classify anomalous conditions. In recent years, there have been many reports of achieving high accuracy in diagnosing abnormalities in buildings and moving objects by using machine learning algorithms to analyze sensor signals.[20–22] On the other hand, few methods have been established for machine learning analysis of sensor signals transmitted from a self-powered system.[23] In this study, we used an air compressor as the monitoring target and acquired the electric power through a vibrational energy harvester (VEH). One of the novel ideas of this study is that the time interval between the amount of generated energy reaching a certain threshold and the transmission of a wireless signal is used in the analysis. On the basis of the accuracy of fault diagnosis, the possibility of a self-powered monitoring system using energy harvesting is discussed.

2. Self-powered Fault Diagnostic System

Figure 1 shows a schematic diagram of our fault diagnosis system using energy harvesting. A piezoelectric bending transducer (MIDE, S128-J1FR-1808YB) was used as the VEH. The transducer includes a piezoelectric Pb(Zr, Ti)O_3 layer with a unimorph structure and is capable of generating a maximum of 10.0 V at a resonant frequency of 134 Hz. Since the air compressor (Takagi, 10L ACP-10A) subject to fault diagnosis had a frequency that oscillated significantly at 25 Hz, a 8.3 g mass was fixed to the tip of the transducer to adjust the resonant frequency to 25 Hz. The VEH was firmly installed in the air compressor via a holder made of acrylonitrile butadiene styrene (ABS). The resulting power was stored in an electrolytic capacitor with a capacitance of C_s after full-wave rectification. When the storage voltage V_c in the capacitor reached 4 V, the DC/DC converter (Analog Devices, LTC3588-1) was activated to output a

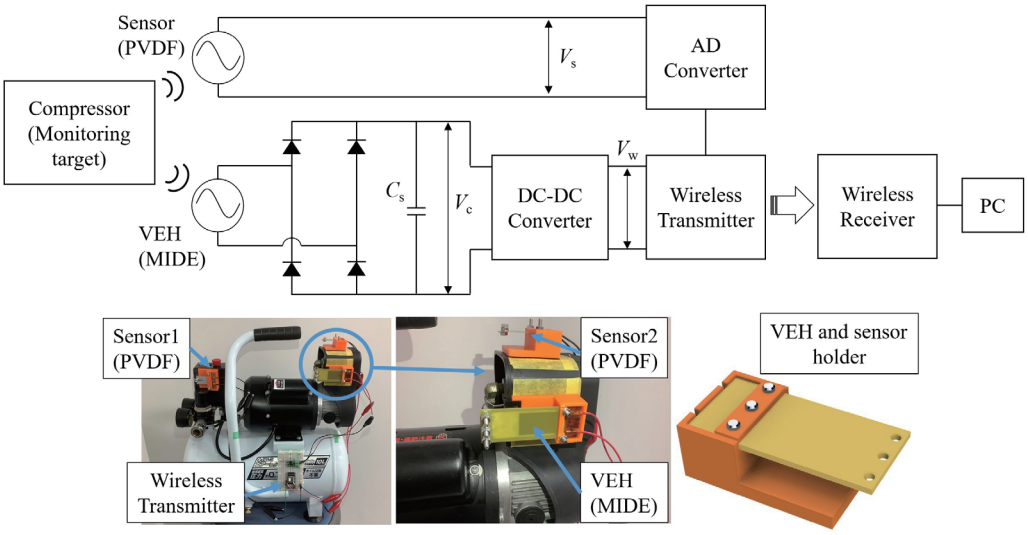

Fig. 1. (Color online) Experimental setup for diagnosing air compressor failure with a VEH and PVDF sensors.

supply voltage V_w of 2.5 V to the wireless transmitter. The wireless transmitter module (Mono Wireless, TWELITE DIP BLUE) complies with IEEE 802.15.4 and uses the 2.4 GHz band for wireless transmission. The generated voltage V_s of the piezoelectric PVDF film (KF piezo film, Kureha) attached to the air compressor as a vibration sensor was measured using an AD converter with a sampling rate of 30 ms. Both the wireless transmitter and AD converter were operated with the VEH as the power source, and the vibration data were acquired using a USB-connectable wireless receiver (Mono Wireless, MONOSTICK). The PVDF film was cut to 35 mm (length) × 17 mm (width) × 40 μm (thickness), and aluminum was vacuum-deposited on the film as electrodes. Then, the film was laminated with PET and adjusted to the resonant frequency of the air compressor by adding a mass, and installed in multiple locations on the air compressor with the ABS holder.

3. Energy Harvesting for Wireless Data Transmission

Figure 2 shows the charging characteristics of the VEH. The VEH was shaken with a shaker (Mitutoyo, MEE15) at a constant amplitude of 25 Hz, and then charged to a capacitor with C_s = 10–2000 μF after full-wave rectification. Figure 2(a) shows transient waveforms of V_c; it can be seen that the time to reach the saturation voltage increases as C_s increases. Since the capacitance of the VEH was 225 nF, the impedance of the storage capacitor was completely mismatched. Therefore, the charging efficiency is low and must be improved in the future through appropriate impedance conversion circuitry. However, we would like to emphasize that the VEH was able to supply sufficient power to the wireless transmitter with a time interval of several tens of seconds with the VEH. The stored energy U_c, which is expressed by

$$U_c = \frac{1}{2} C_s V_c^2, \tag{1}$$

saturated at a value that increased in proportion to C_s as shown in Fig. 2(b). This is because the saturation voltage of V_c is constant. The saturation energy of U_c determined the operating time of the wireless transmitter.

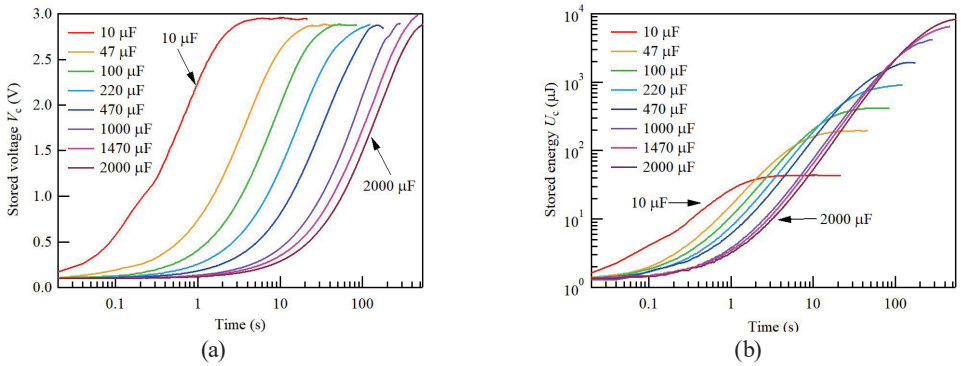

(a) (b)

Fig. 2. (Color online) (a) Transient waveforms of stored voltage V_c and (b) stored energy U_c in capacitors in charging process.

Figure 3 shows the charge–discharge and wireless transmission characteristics of the system shown in Fig. 1 when the DC/DC converter and wireless devices were driven. Figure 3(a) shows the transient waveforms of V_c and supply voltage V_w for the wireless transmitter when C_s = 470 μF. It can be seen that the DC/DC converter and wireless transmitter were operating when V_c reached 4 V. After a rapid decrease in V_c due to the energy consumption of the capacitor, wireless transmission stopped when V_c decreased below 3 V, and then recharging was repeated. Figure 3(b) is an enlarged view of Fig. 3(a), showing that V_w remained constant at 2.5 V while the wireless transmitter continued to operate, and V_c decreased in a stepwise manner. The staggered decrease in voltage corresponds to the fact that each signal with sensor data was transmitted to the wireless receiver at a sampling interval of 30 ms. The maximum number of points that could be transmitted wirelessly at one time depended on C_s, as shown in Fig. 3(c). It was confirmed that wireless transmission was possible for C_s > 80 μF. On the basis of the results, we successfully quantified the relationship between the data transmission interval and the number of data points during the constant monitoring of the air compressor.

4. Fault Diagnosis Based on Machine Learning

For the fault diagnosis of the air compressor, the detection of two abnormal states was targeted in addition to the normal state: an unstable state with a cushion placed under the air

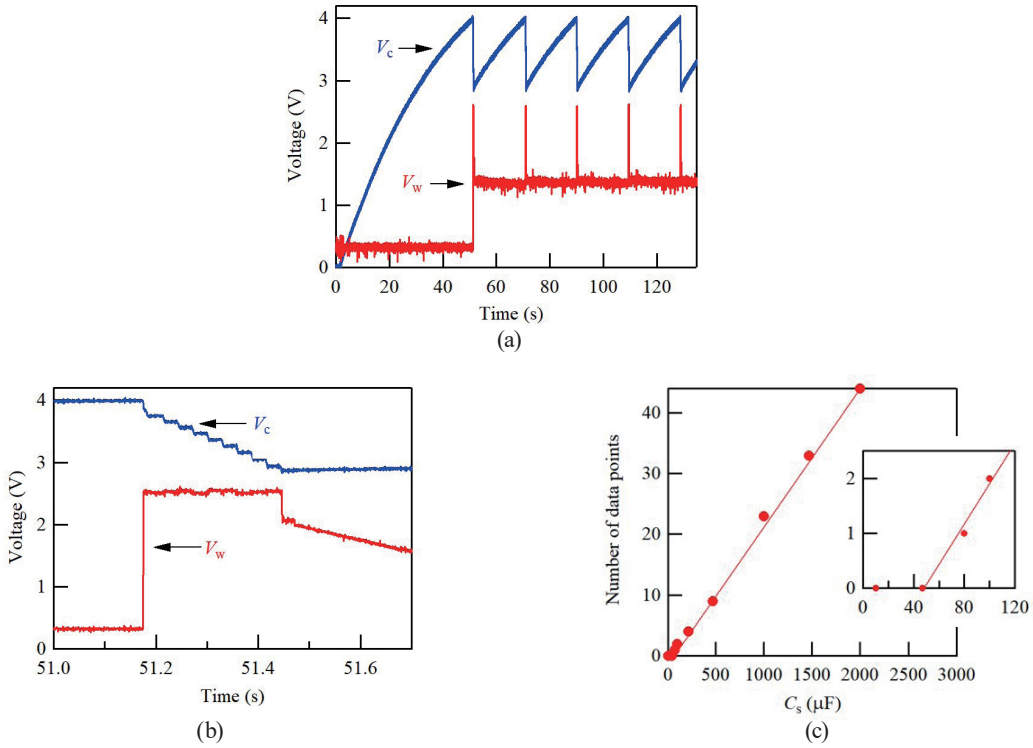

Fig. 3. (Color online) (a) Transient waveforms of stored voltage V_c and supply voltage V_w for wireless transmitter when C_s = 470 μF. (b) Enlarged view of waveform (a). (c) Plot of the number of the transmitted data points against C_s.

compressor and an overturned state in which the compressor fell over on its side. Figure 4 shows the transient waveforms when the sensor voltage signals from two locations of the air compressor were continuously transmitted wirelessly while the capacitor with C_s = 2000 μF was charged with the VEH. The maximum number of data points for periodic wireless transmission was 44 as shown in Fig. 3(c), and furthermore, some data are lost due to errors during wireless transmission. In addition, the entire vibration waveform could not be obtained with a sampling interval of 30 ms. This is evident from the fact that the vibration occurred at multiple resonance frequencies above 25 Hz. The amplitude values of the sensors tended to be larger in the overturned state for both sensors 1 and 2 than in the normal and unstable states. Regarding the intervals during wireless transmissions, the unstable state, where vibration was suppressed, tended to have the longest intervals, while the overturned state tended to have the shortest intervals. These results correspond to the fact that the amount of power generated by the VEH varied with the condition of the air compressor.

The relationship between the average of the absolute value of V_s in one data sequence and the wireless transmission interval t_w is plotted in Fig. 5. The number of data points plotted is 105 for normal, 66 for unstable, and 164 for overturned for sensors 1 and 2. As shown in Fig. 5(a), the distribution of the plot points changed with the state of the air compressor and the sensor position.

On the basis of the results, machine learning was used for state identification and anomaly detection. The *k*-nearest neighbor (*k*NN) algorithm is the one of the simplest methods in supervised classification.[24] The training data are plotted on a vector space, and when unknown data are obtained, any *k* data are obtained from them in order of distance, and the class to which the data belong is estimated by majority vote. Figure 6 shows the accuracy of state identification with the *k*NN algorithm. When the accuracy was verified for each *k* value using t_w and V_s of sensor 1 in the 2D feature space as shown in Fig. 5(b), a high value of approximately 80% was obtained. In the case of using t_w and V_s of sensor 2, a higher accuracy of up to 99% was achieved for state identification. The same accuracy rate was achieved when t_w and V_s of sensors 1 and 2 were all used to discriminate in a 3D feature space. This indicates that the signal at sensor 2 was

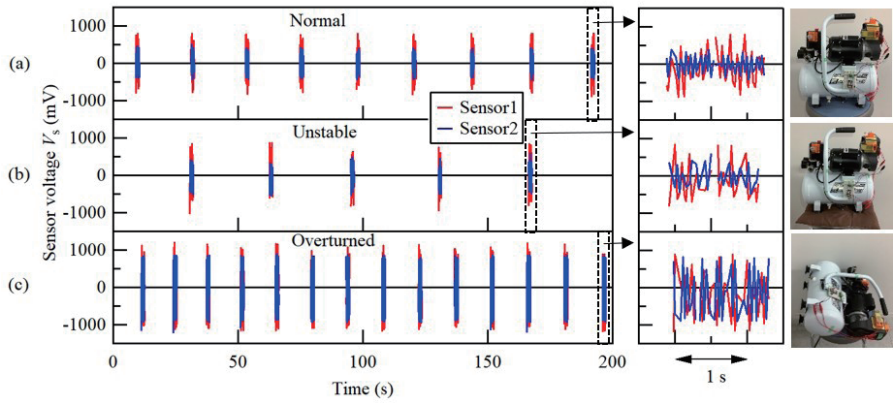

Fig. 4. (Color online) Transient waveforms of typical sensor voltage V_s transmitted from wireless device under (a) normal, (b) unstable, and (c) overturned states of the air compressor.

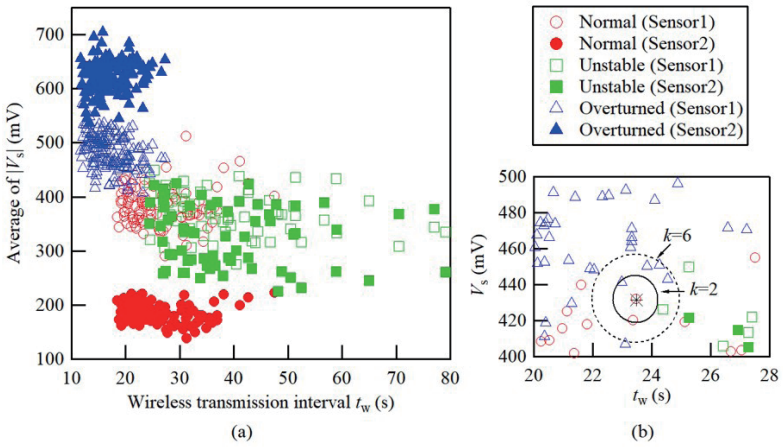

Fig. 5. (Color online) (a) Plots of average of $|V_s|$ against transmitted interval t_w of wireless signal. (b) Enlarged view of plot and classification by *k*NN algorithm.

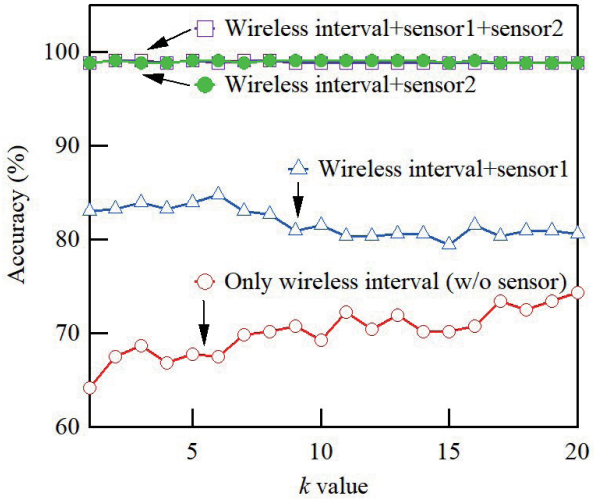

Fig. 6. (Color online) Accuracy of state identification with *k*NN algorithm.

effective in performing state identification with high accuracy. When the identification was performed with only t_w without using the sensor signals, the maximum accuracy was 74% at a k value of 20. This indicates that effective state identification is possible even in extremely low power energy harvesting where only wireless signals can be transmitted without an AD converter. However, when highly accurate state identification is required, the accuracy can be improved by using both the wireless transmission interval and the sensor signal.

The local outlier factor (LOF) algorithm,[24] a type of unsupervised learning, was then used for abnormality detection. In this algorithm, the previously acquired normal condition data are used as the criterion, and the abnormality is scored by comparing the local density with the neighboring points of the data to be diagnosed. Figure 7 shows the accuracy of abnormality

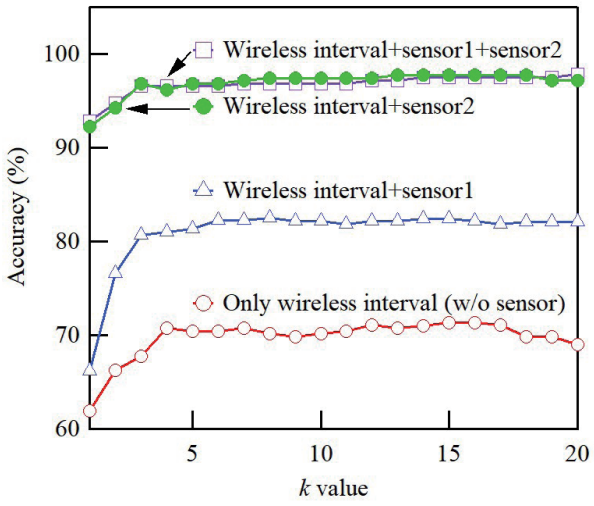

Fig. 7. (Color online) Accuracy of abnormality detection with LOF algorithm.

detection with the LOF algorithm. In this result, the same trend as in the state identification shown in Fig. 6 was obtained, and a maximum of 98% accuracy was obtained when t_w and V_s of sensors 1 and 2 were used. It is clear that the LOF algorithm is effective in diagnosing abnormalities by learning only normal data, even when training data of the failure state are difficult to obtain.

5. Conclusions

In this study, a self-powered fault diagnosis system using vibration energy harvesting was constructed to successfully identify the state of a monitored target and detect abnormalities. By using the *k*NN algorithm as supervised learning, the system was able to identify three states (normal, unstable, and overturned) with a maximum accuracy of 99%. In addition, by using the LOF algorithm as unsupervised learning, abnormality detection with a maximum accuracy of 98% was achieved. One of the factors contributing to the high accuracy of diagnosis was the addition of the wireless transmission interval as a machine learning feature, noting that the amount of energy generated by the VEH depended on the state of the monitored target. Thus, we conclude that not only can energy harvesting be utilized as a permanent power supply for a fault diagnostic system, but also that the amount of energy generated can serve as information indicating the state of the target.

Acknowledgments

This work was supported by JST PRESTO Grant Number JPMJPR16R4, Japan; JST CREST Grant Number JPMJCR21Q2, Japan; and JSPS KAKENHI Grant Number 17H04814, Japan.

References

1 H. Akinaga: Jpn. J. Appl. Phys. **59** (2020) 110201. https://doi.org/10.35848/1347-4065/abbfa0
2 S. Zelenika, Z. Hadas, S. Bader, T. Becker, P. Gljušćić, J. Hlinka, L. Janak, E. Kamenar, F. Ksica, T. Kyratsi, L. Louca, M. Mrlik, A. Osmanović, V. Pakrashi, O. Rubes, O. Ševeček, J. P. B. Silva, P. Tofel, B. Trkulja, R. Unnthorsson, J. Velagić, and Ž. Vrcan: Sensors **20** (2020) 1. https://doi.org/10.3390/s20226685
3 X. Li, L. Teng, H. Tang, J. Chen, H. Wang, Y. Liu, and M. Fu: IEEE Internet Things J. **8** (2021) 1728. http://doi.org/10.1109/JIOT.2020.3016993
4 M. Zhu and E. Worthington: Proc. IEEE Sensors (2009) 699. https://doi.org/10.1109/ICSENS.2009.5398559
5 S. P. Beeby, M. J. Tudor, and N. M. White: Meas. Sci. Technol. **17** (2006) R175. https://doi.org/10.1088/0957-0233/17/12/R01
6 T. Ueno: AIP Adv. **9** (2019) 035018. https://doi.org/10.1063/1.5079882
7 H. Toshiyoshi, S. Ju, H. Honma, C.-H. Ji, and H. Fujita: Sci. Technol. Adv. Mater. **20** (2019) 124. https://doi.org/10.1080/14686996.2019.1569828
8 S. Priya, H.-C. Song, Y. Zhou, R. Varghese, A. Chopra, S.-G. Kim, I. Kanno, L. Wu, D. S. Ha, J. Ryu, and R. G. Polcawich: Energy Harvest Syst. **4** (2017) 3. https://doi.org/10.1515/ehs-2016-0028
9 T. Mori: Small **13** (2017) 1702013. https://doi.org/10.1002/smll.201702013
10 N. Jaziri, A. Boughamoura, J. Müller, B. Mezghani, F. Tounsi, and M. Ismail: Energy Rep. **6** (2020) 264. https://doi.org/10.1016/j.egyr.2019.12.011
11 D. Champier: Energy Convers. Manag. **140** (2017) 167. https://doi.org/10.1016/j.enconman.2017.02.070
12 C. S. Psomopoulos: Handbook of Sustainable Engineering, Eds. J. Kauffman, K.-M. Lee (Springer Netherlands, 2013) p. 1065. https://doi.org/10.1007/978-1-4020-8939-8_117
13 L. Sucupira and J. Castro-Gomes: CivilEng **2** (2021) 852. https://doi.org/10.3390/civileng2040046
14 F. Sangoleye, N. Irtija, and E. E. Tsiropoulou: Sensors **21** (2021) 2755. https://doi.org/10.3390/s21082755
15 G. Charalampidis, A. Papadakis, and M. Samarakou: Energy Procedia **157** (2019) 892. https://doi.org/10.1016/j.egypro.2018.11.255
16 M. K. Mishu, M. Rokonuzzaman, J. Pasupuleti, M. Shakeri, K. S. Rahman, F. A. Hamid, S. K. Tiong, and N. Amin: Electronics **9** (2020) 1. https://doi.org/10.3390/electronics9091345
17 Y. Fang, T. Tang, Y. Li, C. Hou, F. Wen, Z. Yang, T. Chen, L. Sun, H. Liu, and C. Lee: iScience **24** (2021) 102300. https://doi.org/10.1016/j.isci.2021.102300
18 M. Zareei, C. Vargas-Rosales, M. H. Anisi, L. Musavian, R. Villalpando-Hernandez, S. Goudarzi, and E. M. Mohamed: Energies **12** (2019) 2794. https://doi.org/10.3390/EN12142794
19 F. U. Khan and I. Ahmad: Shock Vib. **2016** (2016) 1340402. https://doi.org/10.1155/2016/1340402
20 Y. Ren: ASCE-ASME J. Risk Uncertain. Eng. Syst. B **7** (2021) 1. https://doi.org/10.1115/1.4049525
21 M. H. Mohd Ghazali and W. Rahiman: Shock Vib. **2021** (2021) 9469318. https://doi.org/10.1155/2021/9469318
22 Y. Yang, M. M. M. Haque, D. Bai, and W. Tang: Energies **14** (2021) 7017. https://doi.org/10.3390/en14217017
23 J. Wang, D. Yurchenko, G. Hu, L. Zhao, L. Tang, and Y. Yang: Appl. Phys. Lett. **119** (2021) 100502. https://doi.org/10.1063/5.0063488
24 Y. Lei, B. Yang, X. Jiang, F. Jia, N. Li, and A. K. Nandi: Mech. Syst. Signal Process. **138** (2020) 106587. https://doi.org/10.1016/J.YMSSP.2019.106587